# Adaptable microfluidic system for single-cell pathogen classification and antimicrobial susceptibility testing

Hui Li[a], Peter Torab[b], Kathleen E. Mach[c], Christine Surrette[d], Matthew R. England[e], David W. Craft[e], Neal J. Thomas[f,g], Joseph C. Liao[c], Chris Puleo[d], and Pak Kin Wong[a,b,h,1]

[a]Department of Biomedical Engineering, The Pennsylvania State University, University Park, PA 16802; [b]Department of Mechanical Engineering, The Pennsylvania State University, University Park, PA 16802; [c]Department of Urology, Stanford University School of Medicine, Stanford, CA 94305; [d]Electronics Organization, GE Global Research, Niskayuna, NY 12309; [e]Pathology and Laboratory Medicine, Penn State Milton S. Hershey Medical Center, Hershey, PA 17033; [f]Department of Pediatrics, College of Medicine, The Pennsylvania State University, Hershey, PA 17033; [g]Department of Public Health Sciences, College of Medicine, The Pennsylvania State University, Hershey, PA 17033; and [h]Department of Surgery, College of Medicine, The Pennsylvania State University, Hershey, PA 17033

Edited by David A. Weitz, Harvard University, Cambridge, MA, and approved April 2, 2019 (received for review November 15, 2018)

**Infectious diseases caused by bacterial pathogens remain one of the most common causes of morbidity and mortality worldwide. Rapid microbiological analysis is required for prompt treatment of bacterial infections and to facilitate antibiotic stewardship. This study reports an adaptable microfluidic system for rapid pathogen classification and antimicrobial susceptibility testing (AST) at the single-cell level. By incorporating tunable microfluidic valves along with real-time optical detection, bacteria can be trapped and classified according to their physical shape and size for pathogen classification. By monitoring their growth in the presence of antibiotics at the single-cell level, antimicrobial susceptibility of the bacteria can be determined in as little as 30 minutes compared with days required for standard procedures. The microfluidic system is able to detect bacterial pathogens in urine, blood cultures, and whole blood and can analyze polymicrobial samples. We pilot a study of 25 clinical urine samples to demonstrate the clinical applicability of the microfluidic system. The platform demonstrated a sensitivity of 100% and specificity of 83.33% for pathogen classification and achieved 100% concordance for AST.**

infection | diagnostics | antimicrobial susceptibility testing | single-cell analysis | microfluidics

Bacterial infection is a leading cause of morbidity and mortality and accounts for over $20 billion in healthcare costs in the United States each year (1–3). Current diagnostic methods for bacterial infection typically involve transport of patient samples to a clinical microbiology laboratory where a bacterial culture procedure, such as agar plate, blood tube, or sputum culture, is performed to test for the presence of bacterial pathogens. Morphological, biochemical, and molecular assays are used to identify the species and perform antimicrobial susceptibility testing (AST) (4–6). These culture-based assays typically require 3–5 d. Without microbiological analysis, physicians often resort to prescribing broad-spectrum antibiotics based on the worst-case assumption of the most virulent bacteria (7, 8). This practice results in improper and unnecessary treatment, disruption of the patients' microbial makeup, poor clinical outcomes, and the emergence of multidrug-resistant pathogens (9). Rapid microbiological analysis techniques are essential to properly manage infectious diseases and combat multidrug-resistant pathogens (10–12).

Phenotypic culture is the current standard in clinical microbiology. Colony morphology (form, elevation, and appearance), gram stain, and biochemical phenotyping are culture-based techniques to classify and identify the bacteria. Molecular approaches, such as multiplex PCR and mass spectroscopy, can be performed with isolated bacteria to identify strains (13–17). To determine the antimicrobial resistance of the pathogen, the growth of the pathogen in the presence of antibiotics is interpreted and reported for therapeutic management of the patient (18–21). Recently, biosensor platforms, including optical, electrochemical, loop-mediated isothermal amplification, and biophysical biosensors, have been developed to detect bacterial growth for AST (22–33). To improve sensitivity and accelerate AST, microfluidic approaches, such as digital microfluidics, agarose microchannels, electrokinetics, and microfluidic confinement, have been demonstrated for performing AST at the single-cell level (34–41). In particular, physical confinement of the pathogen allows rapid AST on a time scale comparable to the doubling time of the bacteria (40, 41). Nevertheless, these techniques neither provide information about the bacterial species nor distinguish polymicrobial samples (42). Furthermore, most existing techniques require cultured isolates and are optimized based on a small panel of pathogens, thereby limiting their general applicability for infectious disease diagnostics.

In this study, we develop an adaptable microfluidic system that determines the presence of bacterial pathogens, classifies the species based on their physical features, and performs phenotypic AST at the single-cell level. In particular, an adaptable microchannel with tunable pneumatic valves physically traps bacteria and classifies the bacterial species according to their physical size and shape in as little as 3 min. It can guide the selection of appropriate antibiotic candidates in the subsequent susceptibility testing. By monitoring growth of individual bacteria in the presence of an antibiotic, antimicrobial resistance can be determined rapidly. We evaluate the performance of the adaptable

## Significance

**Drug-resistant pathogens are one of the major global health risks. However, conventional antimicrobial susceptibility testing (AST) approaches, which typically rely on overnight culture to isolate bacteria, require 3–5 days. Despite rapid pathogen identification techniques having been developed, the ability to rapidly determine bacteria susceptibility represents an unmet need in clinical microbiology. Existing rapid AST techniques are often designed based on a small panel of bacteria and the system neither provides information about the bacterial species nor distinguishes polymicrobial samples. By incorporating an adaptable microfluidic design, we demonstrate a phenotypic AST system that rapidly determines the existence of bacteria, classifies major classes of bacteria, detects polymicrobial samples, and identifies antimicrobial susceptibility directly from clinical samples at the single-cell level.**

Author contributions: H.L., P.T., C.P., and P.K.W. designed research; H.L., P.T., and M.R.E. performed research; M.R.E., D.W.C., and N.J.T. contributed new reagents/analytic tools; H.L., P.T., K.E.M., C.S., D.W.C., N.J.T., J.C.L., C.P., and P.K.W. analyzed data; and H.L., J.C.L., and P.K.W. wrote the paper.

The authors declare no conflict of interest.

This article is a PNAS Direct Submission.



[1]To whom correspondence should be addressed. Email: pak@engr.psu.edu.

This article contains supporting information online at www.pnas.org/lookup/suppl/doi:10.1073/pnas.1819569116/-/DCSupplemental.

Published online May 8, 2019.

microfluidic system using clinical isolates, blood cultures, urine, and whole blood samples. To evaluate the clinical feasibility of the microfluidic system for rapid pathogen classification and AST at the single-cell level, 25 clinical samples with blinded pathogens were tested.

## Results

**Design of the Adaptable Microfluidic System.** The adaptable microfluidic design consists of parallel trapping channels under a second layer of pneumatic control channels, which regulate the height of the trapping channel for adapting to various bacteria (*SI Appendix*, Fig. S1). The loading process is based on real-time monitoring of bacteria trapped in the channel (Fig. 1*A* and *SI Appendix*, Fig. S2 *A* and *B*). In the experiment, a sample of 20 μL was loaded in the inlet of the microfluidic system and filled the channel due to capillary force. As evaporation occurred at the outlet, the bacteria were continuously driven into the channels. Evaporation also occurred at the inlet, which gradually concentrated the sample. With a large pressure (e.g., 200 kPa), bacteria were trapped at the entrance of the observation window, which determined the presence of bacteria. To estimate the size of the bacteria, the pressure was released and the bacteria moved inward into the trapping region with a velocity on the order of 10 μm/s. Pressure was then applied and adjusted to trap the bacteria within the channels. After bacteria loading, culture medium was applied on both sides of the channels to balance the hydrodynamic force and prevented further loading of bacteria.

In this study, at least five bacteria are considered for pathogen classification and AST. For a given sample, the trapping time is increased to capture a sufficient number of bacteria. Using this protocol, we have demonstrated trapping of samples with bacteria from $5 \times 10^3$ to $10^8$ cfu/mL (*SI Appendix*, Fig. S2*C*). For instance, less than 3 min was required to trap a sample with $10^7$ cfu/mL. Tens of bacteria could be trapped in ∼10 min for samples with a concentration of $5 \times 10^5$ cfu/mL [as suggested in the Clinical and Laboratory Standards Institute (CLSI) guidelines] (43). The loading time was increased to 30 min for handling samples with $5 \times 10^3$ cfu/mL. The trapping channels also serve as a physical filter to eliminate large cells and debris in physiological samples. This loading process selectively loads target pathogens into the channels and minimizes clogging issues resulting from the sample matrix (*SI Appendix*, Fig. S2*D*). This loading process examines the predominating species in the sample and inherently avoids false positive results due to flora, which typically has a low concentration.

Confinement and classification of bacteria were performed by pneumatically adjusting the dimensions of the trapping channels (Fig. 1*B*). The channel dimensions and cross-section profile were studied with atomic force microscopy and finite element analysis (*SI Appendix*, Figs. S3 and S4). The height of the trapping

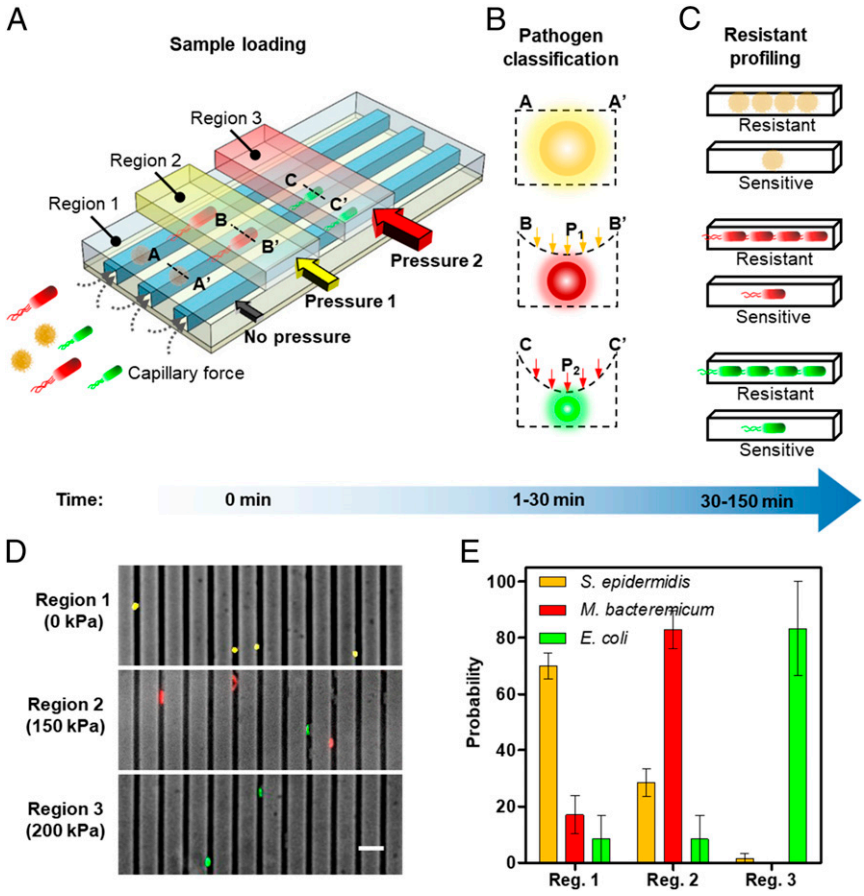


**Fig. 1.** Single-cell pathogen classification and AST. (*A*) Schematic of the adaptable microfluidic device for pathogen classification and AST at the single-cell level. Bacterial pathogens are loaded into the channels automatically by capillary force. (*B*) Cross-section profiles of the channel under different pneumatic pressures. Bacteria are trapped in different regions of the channels and classified according to the applied pressure, which dynamically adjusts the height of the channel. (*C*) Antimicrobial susceptibility is determined by monitoring phenotypic growth of the bacteria in the presence of antibiotics. (*D*) Microfluidic separation of three bacterial species by the tunable microfluidic device. *S. epidermidis*, *M. bacteremicum*, and *E. coli* were fluorescently stained, mixed, and loaded to the microfluidic system to demonstrate the pathogen separation. Images are representative of three independent experiments. (Scale bar, 10 μm.) (*E*) Distributions of the bacteria in regions with 0, 150, and 200 kPa applied pressure in the microchannels. Data represent mean ± SEM ($n = 3$).

channel could be adjusted from 0 to 1.3 μm with a pressure between 300 and 0 kPa. Bacteria are trapped when the channel dimensions match the dimension of the pathogen. This feature enables pathogen classification for species with different physical size. Trapping bacteria in the pneumatic control channel region also facilitates follow-up time-lapse imaging of the bacteria.

Taking advantage of microfluidic confinement, single-cell AST can be performed phenotypically in the presence of antibiotics in the channel. Resistant strains can grow in the presence of the antibiotic while the antibiotic would inhibit the growth of susceptible strains (Fig. 1*C*). As the cross-section of the channels is compatible with the size of the pathogen, the bacterial growth is confined along the microchannel. The change in length of the bacteria in the channel over time is used to quantitatively measure the growth of the bacteria. This approach dramatically reduces the AST time to a time scale comparable to the doubling time of the bacteria.

**Single-Cell Pathogen Classification and AST.** Pathogen classification by the adaptable microfluidic system was first demonstrated using cultured *Escherichia coli*, *Staphylococcus epidermidis*, and *Mycobacterium bacteremicum* (Fig. 1*D* and *SI Appendix*, Fig. S5). These species could be physically separated with different pressure values (i.e., different regions of the microchannel). A calibration experiment was performed to estimate the pressure values (Movies S1–S3). The distribution of the bacteria provided an indication on the size of the species. In the experiment, the majority of *S. epidermidis* (66%), *M. bacteremicum* (83%), and *E. coli* (83%) were trapped in the regions with 0 kPa, 150 kPa, and 200 kPa pneumatic pressure, respectively (Fig. 1*E*).

To understand the trapping process, the physical dimensions of the bacteria were evaluated using scanning electron microscopy (SEM) (Fig. 2 *A*, *D*, and *G*). Since the bacteria were trapped along the channel, we measured the characteristic lengths by the width of rod-shaped cells (bacilli) and diameter for spherical cells (cocci). The characteristic lengths of *S. epidermidis*, *M. bacteremicum*, and *E. coli* were 0.79 ± 0.06, 0.52 ± 0.02, and 0.47 ± 0.04 μm, respectively. The size difference between *M. bacteremicum* and *E. coli* was only 50 nm. Nevertheless, the difference in size of the bacteria was successfully captured based on the spatial distribution with multiple pressure regions. Based on our calibration, the heights of the microchannel were 1.32, 0.64, and 0.42 μm at the corresponding pressures suggesting an inverse correlation between the applied pressure and the size of bacteria trapped. In addition to the characteristic length, other properties of the bacteria were observed to influence the trapping pressure as well. For instance, *S. epidermidis* displayed strong adhesion with the polydimethylsiloxane (PDMS) surface and was often trapped at the entrance region of the channel with 0 kPa pressure. *M. bacteremicum*, in contrast, exhibited a high motility (44) and required a slightly higher trapping pressure. The distribution of the bacteria in the microfluidic system at a given pressure therefore represents a signature resulting from multiple characteristics of the species.

The bacterial trapping channel is also capable of single-cell AST by monitoring the phenotypic growth of the trapped bacteria in the channel. In control experiments without antibiotics, the bacteria grew exponentially along the microchannels (Fig. 2 *B*, *E*, and *H*). In contrast, the bacterial growth was inhibited in the presence of antibiotics at the standard breakpoint concentration suggested by the

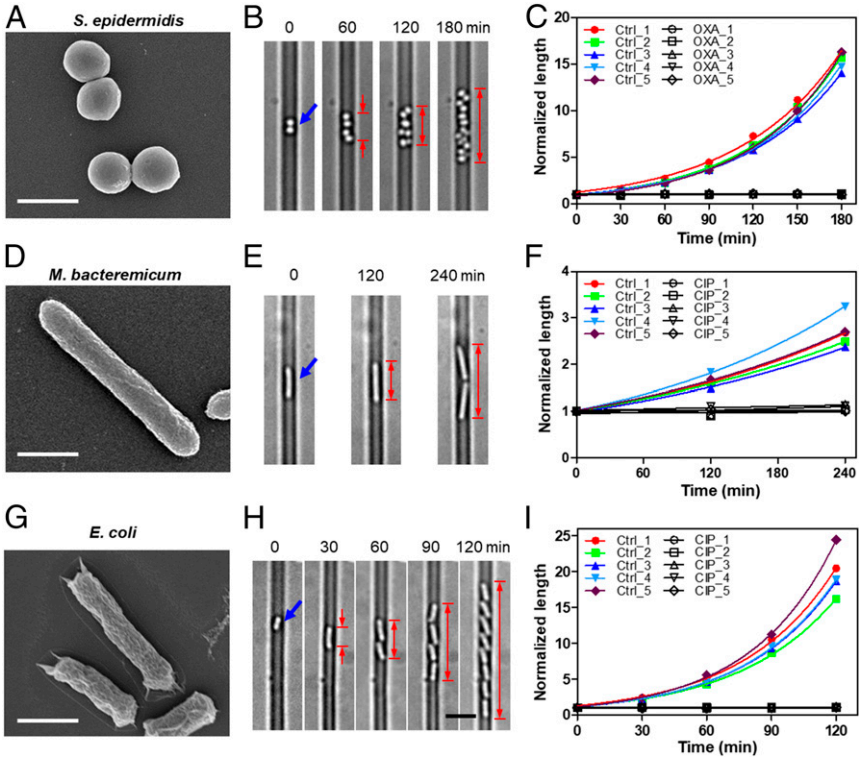


**Fig. 2.** Single-cell AST of different bacterial species. (*A*, *D*, and *G*) Scanning electron microscopy characterization of *S. epidermidis* (diameter = 0.79 ± 0.06 μm, $n = 10$), *M. bacteremicum* (width = 0.52 ± 0.02 μm, $n = 10$), and *E. coli* (width = 0.47 ± 0.04 μm, $n = 10$). (Scale bars, 1 μm.) (*B*, *E*, and *H*) Monitoring growth of single bacteria in the device. Blue arrows indicate the initial positions of the bacteria. Red arrows indicate the length of the bacteria. (Scale bar, 5 μm.) (*C*, *F*, and *I*) Representative growth curves for control (color) and antibiotic (black) groups. Each curve represents growth of a single bacterium. Antimicrobial susceptibility is determined by monitoring phenotypic growth of the bacteria with and without antibiotics. All three bacteria are susceptible to the corresponding antibiotics. Images are representative of five independent experiments.

CLSI guidelines to determine the antimicrobial susceptibility (45). Growth was measured by an increase in the length of the bacteria occupying the microchannel. The length was normalized according to the initial length for estimating the growth rate, to account for variation of the initial length. Comparison of the growth rate between the control experiment and the antibiotic experiment determined the susceptibility of the bacteria. Growth/nongrowth was defined quantitatively by a 50% reduction in the growth rate, which resulted in robust results in our calibration experiments (Fig. 2 *C*, *F*, and *I*). Unless otherwise specified, this definition is applied throughout this study. For instance, ciprofloxacin (CIP) was effective for *E. coli* (EC137) and *M. bacteremicum*, while oxacillin (OXA) completely inhibited the growth of *S. epidermidis*. These results are consistent with broth dilution data, supporting pathogen classification and AST at the single-cell level with the adaptable microfluidic system.

**Identifying Polymicrobial Samples.** This adaptable microfluidic system along with single-cell analysis opens the possibility of identifying polymicrobial infections, which exhibit enhanced disease severity and morbidity. In our experiment, the number of bacteria trapped is counted quantitatively. This capability is essential for identifying polymicrobial samples. We illustrate this capability by testing a sample containing both *E. coli* and *S. epidermidis*. In agreement with our calibration, the majority (80%) of *E. coli* were physically trapped in the region with 180 kPa while the majority (85%) of *S. epidermidis* were trapped in the entrance region with 0 kPa pressure (Fig. 3 *A* and *D*). The separation of these species can be easily verified with the shape. *E. coli* has a rod shape while *S. epidermidis* has a spherical shape (Fig. 3 *B* and *C*). The two species were also discriminated by their antibiotic susceptibility profiles (Fig. 3*E*). In the experiments in the presence of ampicillin (AMP), the *S. epidermidis* strain, which was resistant to AMP, grew exponentially in the microchannels. In contrast, the *E. coli* strain, which was susceptible to ampicillin, was lysed under the same condition. Moreover, bacterial growth rates provided an additional indication of the polymicrobial nature of the sample. In the control

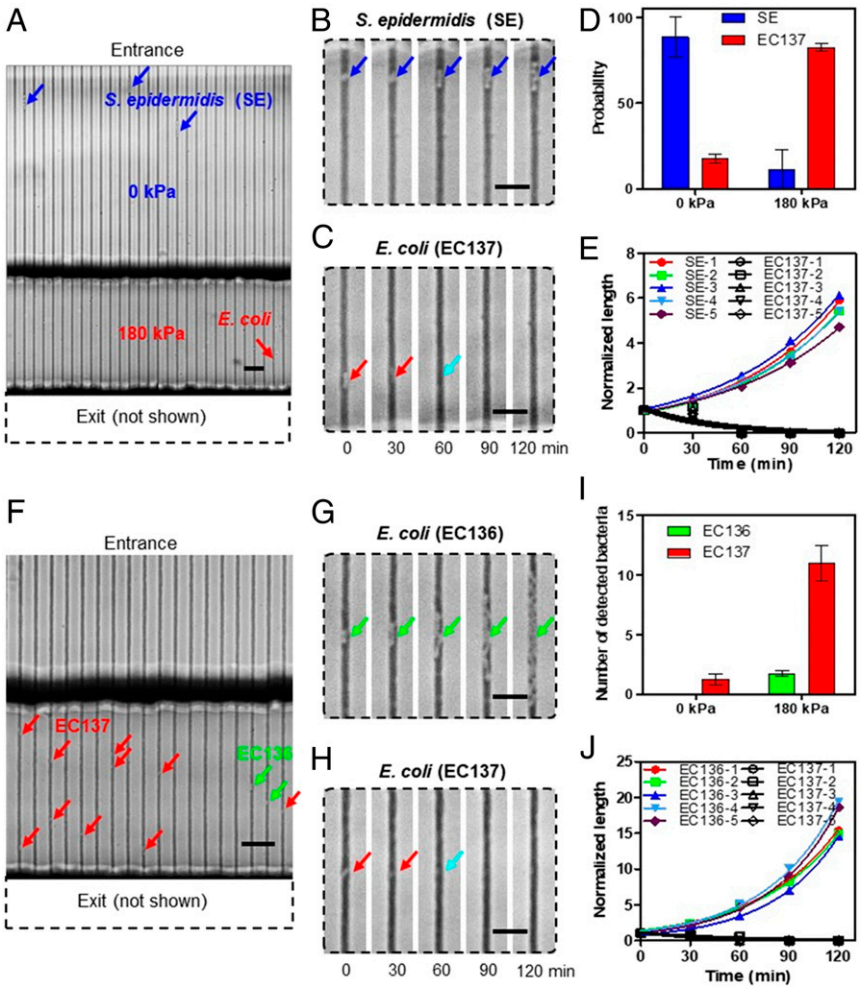


**Fig. 3.** Single-cell AST of polymicrobial samples with the adaptable microfluidic device. (*A*) Identification of polymicrobial samples based on spatial distribution of pathogens. Two bacterial species (*S. epidermidis* at $5 \times 10^5$ cfu/mL and *E. coli* at $5 \times 10^5$ cfu/mL) were trapped in different regions of the channels. (*B* and *C*) Monitoring of bacterial growth in different regions of the channel. Ampicillin (8 μg/mL) displays no effect on *S. epidermidis* and bactericidal effect on the uropathogenic *E. coli* (EC137). (*D* and *E*) Distribution of the bacteria in the channel determined by the antibiotic response of the bacteria. Representative growth kinetics of the two species in the presence of ampicillin in the single-cell AST device. Color symbols represent *S. epidermidis* and black symbols represent *E. coli 137*. (*F*) Identification of polymicrobial samples based on antimicrobial susceptibility. Two strains of *E. coli* (EC137, $5 \times 10^6$ cfu/mL and EC136, $5 \times 10^5$ cfu/mL) were trapped in the same region of the microchannel. (*G* and *H*) EC136 is resistant to ampicillin and grew in the channel. EC137 is susceptible to ampicillin. (*I* and *J*) Distribution of the bacteria in the channel determined by the antibiotic response of the bacteria. Representative growth kinetics of the two strains in the single-cell AST device. Images are representative of three independent experiments. (Scale bars in *A* and *F*, 20 μm; in *B*, *C*, *G*, and *H*, 10 μm.)

experiment without antibiotics, both bacteria grew exponentially in different regions of the microchannels (*SI Appendix*, Fig. S6). Examination of the data revealed that the growth rates were different between the two species. These results support the use of single-cell analysis for identifying samples with multiple species.

We further evaluated the capability of the microfluidic system for identifying samples with multiple strains of the same species, which is challenging for genotypic diagnosis. Two strains of *E. coli* (EC137 and EC136 at a 10:1 ratio) with different antibiotic resistance profiles were tested. EC137 is susceptible to ampicillin while EC136 is resistant to ampicillin. Both strains were trapped in the microchannels at 180 kPa pressure with no spatial separation in the microchannel (Fig. 3*F*). The bacteria strains displayed similar growth rates and were indistinguishable in the control experiments. Nevertheless, examining the antibiotic responses revealed distinct behaviors between the bacteria (Fig. 3 *G*–*I*). In the antibiotic experiment, EC136 grew exponentially with ampicillin in the medium, whereas EC137 was lysed by ampicillin. Fig. 3*J* illustrates the growth curves of EC136 and EC137 in the same experiment. Since EC137 had a higher initial concentration (10-fold over EC136, Fig. 3*I*), this result demonstrated detecting a resistant strain that outgrows a dominating strain over time in the presence of antibiotics (Fig. 3*J*).

**Direct AST with Clinical Samples.** We next evaluated the ability of our device for testing clinical samples, including blood culture (bottle), urine, and whole blood. Single-cell AST was implemented for 10 blood cultures and six urine samples that were cultured positive for the presence of *E. coli*. Blood cultures and urine samples were mixed with Mueller Hinton (MH) broth at a 1:10 ratio and directly loaded in the microfluidic system. Additionally, clinical isolates of *E. coli* were spiked into human whole blood and a pretreatment step was performed to isolate bacteria in the sample before the loading process (*SI Appendix*, Figs. S7 and S8). AST results were determined within 60 min by directly observing the growth of the bacteria in the microfluidic system (Fig. 4*A*). The detailed growth for bacteria in blood cultures was monitored and analyzed at the single-cell level. Among the 10 blood cultures, one (sample 6) was resistant to ciprofloxacin and the others were susceptible (Fig. 4*B*). The growth rate of the resistant bacteria under antibiotic treatment was indistinguishable from the control (i.e., no antibiotic). Similarly, the bacteria in all six urine samples were ciprofloxacin sensitive (Fig. 4*C*). The results were verified by broth dilution with overnight culture (*SI Appendix*, Fig. S9).

The *E. coli*-positive samples allow us to evaluate the influence of the sample variability on the robustness of the system. We studied the effect of the bacterial characteristic length on the trapping process. In our SEM characterization, the width of the *E. coli* strains has a SD of ~40 nm. The pneumatic pressure to trap these *E. coli* strains was 170 ± 17 kPa (mean ± SD, $n$ = 10 independent experiments) (*SI Appendix*, Fig. S10 *A* and *B*). This result indicates that the trapping pressure is consistent for the same strain. We also examined the effect of the source of *E. coli* (i.e., blood or urine) and culture conditions (medium, blood and urine). Comparison of the results from blood, urine, and MH broth suggests the culture condition does not have a significant effect on the trapping pressure for the bacteria (*SI Appendix*, Fig. S10*C*). These results collectively support direct AST of clinical samples with the adaptable microfluidic system.

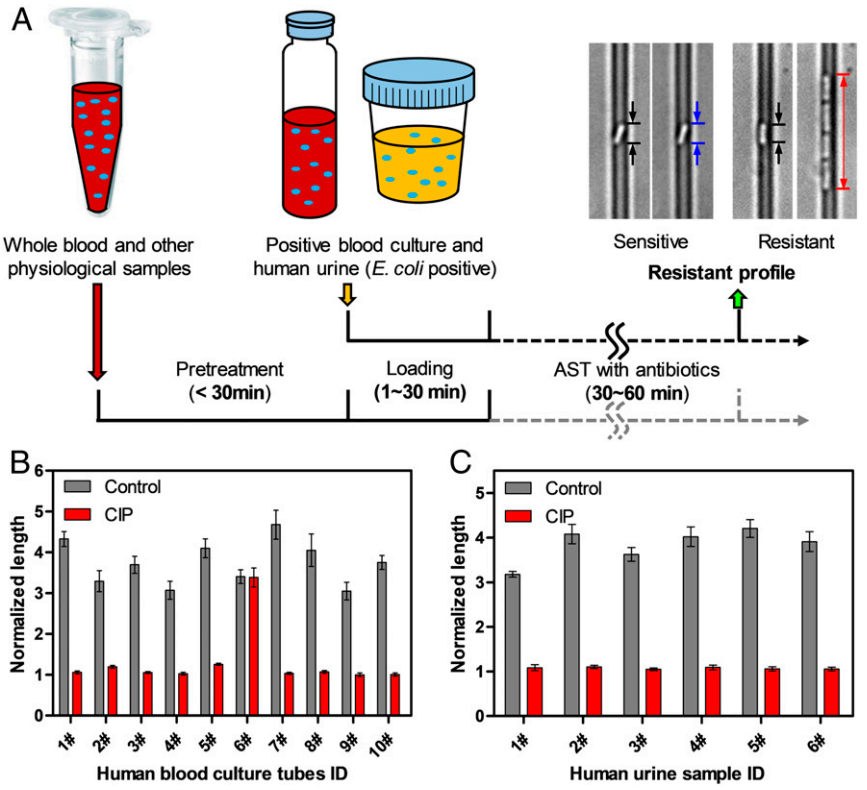


**Fig. 4.** Single-cell AST of clinical samples with the adaptable microfluidic device. (*A*) Single-cell AST procedure for clinical samples. Blood cultures and urine can be mixed with culture medium at a 1:10 ratio with and without antibiotic and loaded directly into the adaptable microfluidic device for single-cell AST. The loading time lies between 1 and 30 min, depending on the bacteria concentration. For whole blood and other physiological samples with complex matrices, sample pretreatment is performed before microchannel loading (as described in *Materials and Methods*). (*B*) Direct AST of 10 positive human blood cultures. Only sample 6 is resistant to ciprofloxacin as confirmed by the clinical microbiology results. (*C*) Direct AST of human urine samples at 60 min. All six samples are susceptible to ciprofloxacin as confirmed by broth dilution.

**Pathogen Classification and AST of Clinical Samples.** We designed a study using clinical urine samples, including negative samples. To classify samples with blinded pathogens (i.e., unknown size), we developed a dynamic protocol to identify the presence and size of bacteria in the samples (Fig. 5*A*). In this protocol, clinical samples were mixed with MH broth and loaded into the microfluidic system. A large pressure (200 kPa) was first applied to trap any bacteria in the samples. For negative samples, the test was repeated three times to verify the result. If a pathogen was identified, the pressure was released and then gradually increased to determine the minimum trapping pressure for pathogen classification. The protocol was repeated to identify bacteria with smaller characteristic lengths in the polymicrobial samples, which could pass through the trapping window with a smaller pneumatic pressure (e.g., the blue strain in Fig. 5*A*). In this study, at least five bacteria were trapped and classified based on the size (minimum trapping pressure) and shape (bacillus and coccus).

The bacteria were classified into *Staphylococcus*-like, *Enterococcus*-like, *Pseudomonas*-like, *Klebsiella*-like, and *E. coli*-like groups. This classification covers most common pathogens that cause urinary tract infections (UTIs). The correlation between the trapping pressure and the characteristic lengths of common uropathogens was validated based on electron microscopy from our experiment and the literature (*SI Appendix*, Fig. S11). A calibration experiment was also performed for determining the threshold values for pathogen classification (*SI Appendix*, Fig. S12). The bacteria were first trapped in the adaptable microfluidic system and classified based on the shape (rod shaped or spherical) (*SI Appendix*, Fig. S12*A*). We classified the shape of the bacteria based on the aspect ratio (length/width) (*SI Appendix*, Fig. S12 *B* and *C*). The aspect ratio of all rod-shaped bacteria was above 2. For instance, *Staphylococcus aureus* has an aspect ratio of ∼1. In contrast, the width and length of *E. coli* are 0.47 and 2 μm, which results in an aspect ratio of ∼4. Then, the minimum trapping pressure was determined for each type of bacteria by performing the dynamic trapping protocol. Due to the natural variation in the size of the bacteria, we defined the minimum trapping pressure as the smallest pressure that trap over 75% of bacteria. For spherical bacteria, the minimum trapping pressure for *S. aureus* was 0 kPa, while *Enterococcus faecium* and the *Enterococcus faecalis* (*Enterococcus* spp.) were trapped at 104 ± 9 and 117 ± 13 kPa (mean ± SD), respectively (*SI Appendix*, Fig. S12*D*). *E. faecium* and *E. faecalis* were classified into an *Enterococcus*-like group (no significant differences were observed). For spherical bacteria (coccus), *Staphylococcus*-like and *Enterococcus*-like groups were separated based on a threshold value of 50 kPa (*SI Appendix*, Fig. S12*D*, red dotted line). For rod-shaped bacteria, *Pseudomonas aeruginosa*, *Klebsiella pneumoniae*, and *E. coli* were trapped at 76 ± 14, 116 ± 12, and 170 ± 17 kPa

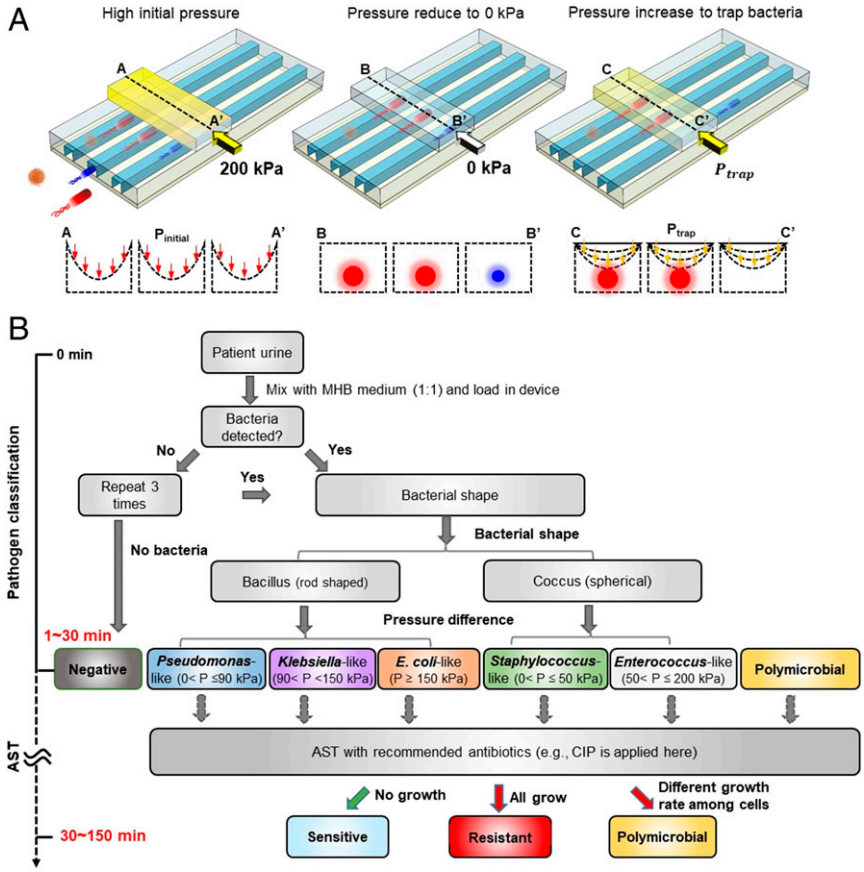


**Fig. 5.** Procedure for single-cell AST of clinical samples with unknown bacteria. (*A*) Schematic view of the single-cell AST procedure for clinical samples with blinded bacteria and the corresponding cross-section profiles of the bottom channels. A high pressure (200 kPa) is first applied to confirm the existence of bacteria in the sample. Then, the applied pressure is released and gradually increased from zero to identify the minimum trapping pressure for pathogen classification. (*B*) Procedure to identify bacteria species in clinical samples with blinded pathogens. Samples are first confirmed for the presence of bacteria. Positive samples are characterized based on the shape (rod or spherical) and size (minimum trapping pressure) for pathogen classification. Five groups, *Staphylococcus*-like, *Enterococcus*-like, *Pseudomonas*-like, *Klebsiella*-like, and *E. coli*-like, are classified. AST is performed in the same microfluidic device. Polymicrobial samples are identified based on pathogen classification and antimicrobial susceptibility.

(mean ± SD), respectively (*SI Appendix*, Fig. S12*E*). These rod-shaped bacteria were classified into *Pseudomonas*-like, *Klebsiella*-like, and *E. coli*-like groups based on threshold values of 90 kPa and 150 kPa (*SI Appendix*, Fig. S12*E*, blue and cyan dotted lines).

In this protocol, the sample was reported as polymicrobial if multiple bacterial populations were identified. The adaptable microfluidic system determines polymicrobial samples by size, shape, growth rate, and antimicrobial susceptibility (Fig. 3). If the bacteria have similar size, shape, growth rate, and antimicrobial susceptibility, the microfluidic system will not be able to discriminate them. Flora and contamination were not considered if the species had a low concentration. For positive samples, the pathogens were cultured with and without ciprofloxacin. To avoid false negatives due to pathogens with a long doubling time, the bacteria were cultured for up to 2 h and the growth rates were compared between samples with and without antibiotic. The pathogen was classified as susceptible when the growth rate was significantly inhibited (i.e., less than half of the control groups) or resistant when the growth rate was similar to the no antibiotic control (i.e., more than half of the control).

In this pilot study, 25 clinical urine samples were tested using the adaptable microfluidic system. The presence of bacteria and the minimum trapping pressure were recorded for each sample (*SI Appendix*, Table S1). Using the adaptable microfluidic system, 19 samples were identified with a single species of bacteria and sample 3 was polymicrobial. Samples 7, 8, 10, 20, and 24 were negative. The samples were independently tested and identified in the clinical microbiology laboratory at Penn State Milton S. Hershey Medical Center. Based on the clinical report, there were four negative samples (samples 7, 8, 20, and 24), 19 monomicrobial samples, one polymicrobial sample (sample 3), and one sample with mixed flora (*SI Appendix*, Table S2). The minimum trapping pressure was compared with the characteristic length of the bacteria (Fig. 6*A*). In agreement with our calibration, the results revealed an inverse relationship and demonstrated a separation resolution below 100 nm. For instance, *Klebsiella* strains (0.56 μm) could be separated from *E. coli* (0.47 μm) despite the small difference in size (<100 nm).

For pathogen classification, most of the samples, including the polymicrobial sample, were correctly classified based on their morphology and the trapping pressure (Fig. 6*B* and *SI Appendix*, Table S2). In particular, the pathogens in polymicrobial sample 3 displayed different shapes (bacillus vs. coccus) and were trapped at different pressure values (*SI Appendix*, Fig. S13). Sample 16 was reported as mixed flora from the microbiology laboratory and was classified as *E. coli* in the microfluidic system. Samples 1 and 6 were misclassified as *Klebsiella*-like in the microfluidic systems. Nevertheless, CHROMagar results suggested that samples 1 and 6 contained only *Klebsiella* spp, suggesting other errors may contribute to the discrepancy. Furthermore, sample 10 reported as *Enterobacter cloacae* in the clinical microbiology laboratory appeared negative in the microfluidic system. Plate counting and MH broth culture also showed sample 10 was negative. The transportation and handling process may potentially introduce error, which may contribute to the discrepancy between the clinical microbiology laboratory and CHROMagar (46, 47). Nevertheless, we do not rule out the possibility that other sources of error may contribute to the discrepancy.

Compared with the results from the clinical microbiology laboratory, the microfluidic system correctly predicted the existence of bacteria for 96% of the samples. The classification approach yields sensitivity of 94.44%, specificity of 57.14%, positive predictive value of 85%, and negative predictive value of 80% (*SI Appendix*, Table S3). Compared with the CHROMagar results obtained at the same site, which avoids transportation and handling errors, the microfluidic system correctly predicted the existence of bacteria for all samples. The classification approach yields sensitivity of 100%, specificity of 83.33%, positive predictive value of 95%, and negative predictive value of 100% (*SI Appendix*, Table S3). AST was performed in the positive samples. In the control experiments, all trapped bacteria grew exponentially over time. The susceptibility profiles were determined by the normalized growth of control groups and antibiotic groups at 2 h (Fig. 6*C*). For samples with a single species, 7 samples were resistant (samples 6, 9, 12, 15, 18, 22, and 25), and 12 samples were sensitive. Similar growth behaviors were observed in the clinical urine experiment, where the growth rates of resistant samples were similar with and without antibiotic. For polymicrobial sample 3, both bacteria were susceptible to ciprofloxacin. Representative growth curves for susceptible, resistant, and polymicrobial samples are shown in Fig. 6 *C*–*F*. These results were in 100% agreement with AST by broth dilution.

## Discussion

In this study, we demonstrate an adaptable microfluidic system that rapidly determines the existence of bacteria, classifies major classes of bacteria, detects polymicrobial samples, and performs phenotypic AST at the single-cell level. The microfluidic system is capable of trapping pathogens with unknown size. The variability in the dimensions of individual bacteria is captured either by the spatial distribution with multiple pressure regions (i.e., regions of multiple microchannel heights; Fig. 1) or adjusting the pressure dynamically (i.e., changing the microchannel heights over time; Fig. 5). The adaptable microfluidic approach separates bacteria according to size and shape and identifies samples with multiple pathogens for polymicrobial infection detection. Compared with other AST approaches, it identifies antimicrobial susceptibility directly from clinical samples with unknown pathogens. The microfluidic system is capable of handling clinical samples, such as human urine and blood cultures. Importantly, the assay times for pathogen classification and AST can be as short as 30 min for *E. coli* and 60 min for *S. epidermidis*, which are the approximate doubling times of the bacteria in our experimental condition.

An important consideration of the adaptable microfluidic system is the sample loading process. In particular, the bacteria are driven into the channels by capillary flow, which can be implemented relatively easily and does not require supporting equipment, such as a pump or a pressure source. The microfluidic channel also serves as a physical filter to selectively load bacterial pathogens into the observation area and facilitate single-cell analysis. Nevertheless, the loading process handles a relatively small volume (~20 μL) and the loading time depends on the bacterial concentration. For instance, it takes less than 3 min for samples with $10^7$ and almost 30 min for samples with a low concentration (e.g., $10^3$–$10^4$ cfu/mL). Using the current design protocol, we have demonstrated trapping of samples with bacteria from $5 \times 10^3$ to $10^8$ cfu/mL (*SI Appendix*, Fig. S2*C*). This range covers the concentration relevant for UTI diagnostics. To provide accurate quantitation for samples with a large range of concentrations and identify flora contamination, the number of channels should be increased to handle numerous bacteria with a larger volume of each sample in the future. Furthermore, sample interfaces, integrated microfluidic concentrator, and real-time, automated imaging analysis techniques should be incorporated into the microfluidic system to automate the sample loading process and improve the quantification accuracy.

We demonstrate the adaptable microfluidic system using blinded clinical urine samples. One of the goals of our approach is to rapidly determine the presence of bacteria at a clinically relevant concentration. Urine is the most common specimen sent to a clinical microbiology laboratory, yet up to 75% of these specimens are negative. A rapid urine test capable of ruling out or confirming the presence of bacteria at a clinically relevant concentration could improve patient care and clinical laboratory workflow. The system also classifies the bacteria based on the

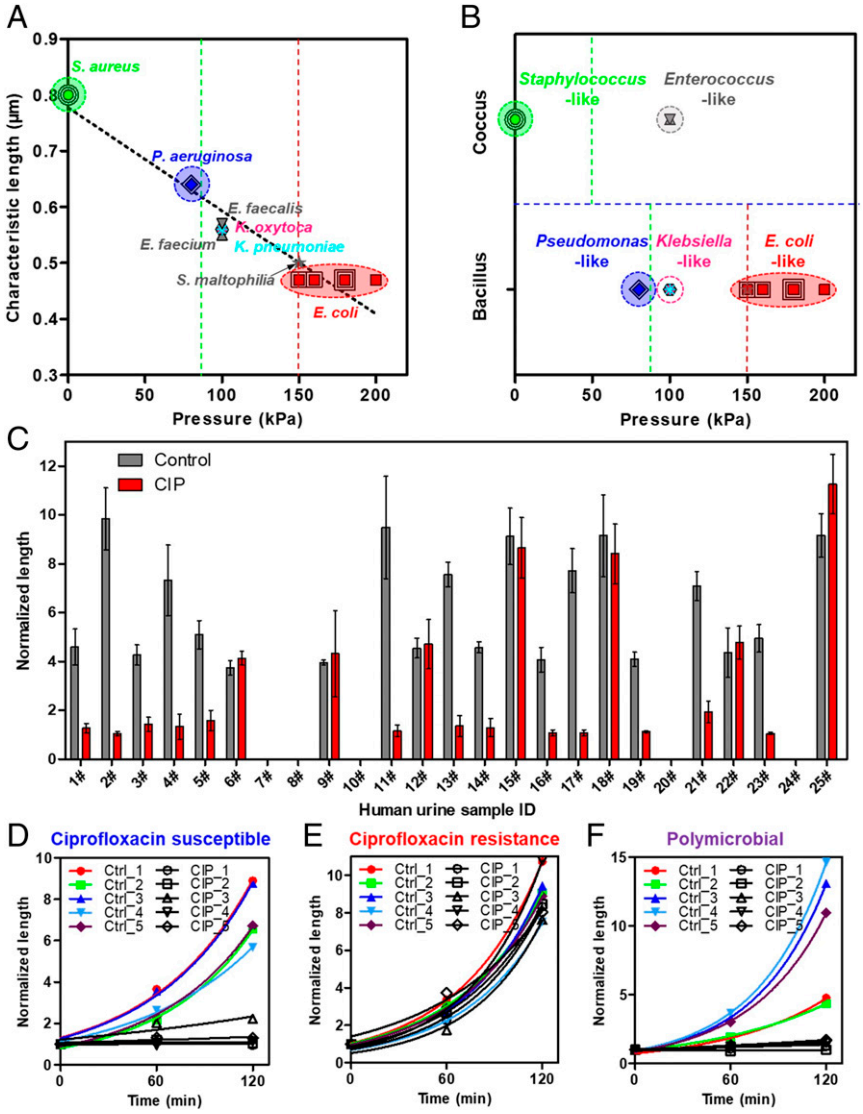


**Fig. 6.** Single-cell AST of clinical urine samples. (*A*) Pathogen identification and AST were performed for 25 clinical urine samples with blinded pathogens. The minimum trapping pressure was compared with the bacterial size of all positive samples, retrospectively. (*B*) Bacteria were classified based on the shape (blue dotted lines) and the minimum trapping pressure (green and red dotted lines). (*C*) Susceptibility was determined for all positive samples at 120 min. Samples 7, 8, 10, 20, and 24 were culture negative. Samples 6, 9, 12, 15, 18, 22, and 25 were ciprofloxacin resistant, as confirmed by broth dilution. (*D*–*F*) Representative growth curves for control groups (color) and antibiotic groups (black) in ciprofloxacin-susceptible sample (*D*, sample 4), ciprofloxacin-resistant sample (*E*, sample 15), and polymicrobial infection sample (*F*, sample 3). In this polymicrobial infection sample, both bacteria (*S. aureus* and *Stenotrophomonas maltophilia*) were susceptible to ciprofloxacin. All curves were fitted with the exponential growth equation in GraphPad Prism.

size and shape. The classification scheme in this study (i.e., *Staphylococcus*-like, *Enterococcus*-like, *Pseudomonas*-like, *Klebsiella*-like, and *E. coli*-like) is tailored to identify the most common pathogens of UTI. In particular, *E. coli* is the cause of most community-acquired and healthcare-associated UTIs. Basic classification of the predominant pathogen in a sample can assist in the selection of appropriate antibiotics for susceptibility testing or treatment and/or of a panel of molecular probes (e.g., PCR primers or hybridization probes) for more precise speciation. Of significance for therapeutic intervention is that AST of the bacteria can be determined in as little as 30 min using the adaptable microfluidic system. Classification of other rod-shaped bacteria (bacillus), such as *K. pneumoniae* and *P. aeruginosa*, is critical for UTI diagnostics, since these bacteria may be treated with different antibiotics compared with *E. coli* due to their high rates of antimicrobial resistance. Identifying *Staphylococcus* spp. and *Enterococcus* spp. will also provide clinically useful information, since these gram-positive bacteria are common causes of UTI and require different treatment options. In the future, further clinical studies with an extended panel of diverse bacterial pathogens and antimicrobial susceptibility profiles should be performed for evaluating the clinical utility of this microfluidic system.

## Materials and Methods

**Bacterial Strains.** There are four bacterial strains included in this study. The *S. epidermidis* (ATCC 12228) and *M. bacteremicum* (ATCC 25791) are from American Type Culture Collection (ATCC). Uropathogenic *E. coli* (EC137 and EC136) were isolated from patient urine samples.

**Clinical Samples.** Deidentified clinical samples were obtained from the clinical microbiology laboratory of the Penn State Milton S. Hershey Medical Center. The procedure was approved by the Pennsylvania State University Institutional Review Board. *E. coli*-positive blood cultures ($n = 10$) and urine samples ($n = 6$) were mixed with MH broth at a ratio of 1:10 with and without ciprofloxacin (4 μg/mL). A total of 25 clinical urine samples with blinded

pathogens were examined using CHROMagar and the microfluidic system. The results were compared with clinical microbiology culture results. These samples were mixed with MH broth at a ratio of 1:1 with and without ciprofloxacin (4 μg/mL). Some samples were stored with glycerol (25% vol/vol) at −80 °C and preincubated for 30 min at 37 °C before use. The bacterial morphology was visually examined with optical microscopy (20× or 40× objective).

**Reagents.** Three different antibiotics, including CIP, AMP, and OXA, were employed in this study. The antibiotics were obtained from Sigma-Aldrich. Human whole blood samples were obtained from the Valley Biomedical Products & Services, Inc. Na heparin was applied as the anticoagulant. Fluorescent dyes, SYTO 9, SYTO 85, and Hoechst 33342, were applied for bacterial staining to calibrate the spatial distributions of different bacteria. The dyes were obtained from Thermo Fisher Scientific. Triton X-100 and IGEPAL CA-630 (Sigma-Aldrich) were applied for blood cell lysis. PDMS (Sylgard 184) for channel fabrication was obtained from Dow Corning.

**Microfluidic Device.** A multilayer microfluidic device with tunable channels was developed for rapid pathogen classification and AST. The device was fabricated by bonding two PDMS layers (*SI Appendix*, Fig. S1). The top layer serves as a pneumatic control channel and the channels in the bottom layer trap bacteria for phenotypic culture. The mold for the top layer was fabricated by patterning a SU-8 layer on a silicon wafer. The channel width is 100 μm, and the channel interval is 100 μm. PDMS (at a ratio of 5:1 between prepolymer and cross-linker) was poured on the mold and cured for 1 h at 80 °C. The bottom microchannel mold was fabricated on a silicon wafer using a reactive-ion etching (RIE) process with a patterned photoresist layer. The width of the microchannels is 2.0 μm and the height of the microchannels is 1.32 μm. PDMS (at a ratio of 20:1 between prepolymer and cross-linker) was spin coated on the mold for 5 min at 3,000 rpm and cured for 3 h at 65 °C. The top control channel layer was peeled off and bonded with the bottom microchannel layer after a 5-min air plasma treatment (PDC-001, Harrick Plasma). The device was incubated for 30 min at 65 °C. In addition, the device was bonded with a glass slide after a second air plasma treatment step. Finally, the device was incubated at 80 °C for 5 min. In the experiment, the microfluidic device was loaded on a microscope (Leica DMI4000B) with a thermal stage for real-time monitoring of the bacterial growth. The bacteria in the adaptable microfluidic system were captured by a charge-coupled device camera (SensiCam QE, PCO), and the growth of the bacteria was measured using ImageJ.

**Single-Cell Antimicrobial Susceptibility Testing.** *E. coli*, *S. epidermidis*, and *M. bacteremicum* were cultured in Mueller Hinton broth, nutrient broth, and ATCC medium 1395, respectively. The bacteria were cultured to an optical density at 600 nm ($OD_{600}$) around 0.2 (measured with Nanodrop 2000; Thermo Fisher Scientific) and diluted to $5 \times 10^5$ cfu/mL following the CLSI guidelines. The concentrations of ciprofloxacin for *E. coli* and *M. bacteremicum* were 4 μg/mL and 2 μg/mL, respectively. The concentration of oxacillin for *S. epidermidis* was 4 μg/mL. A 20-μL sample was loaded into the inlet of the microchannel. Culture medium was applied to immerse the whole device. The device was then loaded on a microscope (Leica DMI4000B), thermal stage for real-time monitoring (SensiCam QE, PCO) of the bacterial growth. The length of the bacteria occupying the microchannel was measured in ImageJ (https://imagej.nih.gov/ij/). In this study, the antibiotic resistance was determined as 50% reduction in the growth rate (or twofold difference in growth rate) in the antibiotic group based on the distribution of the growth rate of single cells. In particular, we define the threshold value based on the standard derivation of single-cell growth and *t* statistics (two tailed, unpaired). In our calibration experiments, the SDs of the growth rate were below 25% of the mean (in the worst case scenario). In the calculation, the degree of freedom was 8, since at least five bacteria were used in each group. A 50% reduction in growth rate is equivalent to a *P* value of ∼0.022.

To model the polymicrobial infection with different species, *E. coli* (EC137) and *S. epidermidis* were cultured to $OD_{600}$ around 0.2, mixed at a ratio of 1:1, and diluted to a final concentration of $1 \times 10^6$ cfu/mL with and without ampicillin (8 μg/mL). To mimic the polymicrobial infection with different strains, *E. coli* (EC137 and EC136) were mixed at a ratio of 10:1 and diluted to a final concentration of $5 \times 10^6$ cfu/mL with and without ampicillin.

**Bacteria Detection in Human Whole Blood.** To detect bacteria in whole blood, *E. coli* (EC137) was spiked into human whole blood. The bacteria were cultured to $OD_{600}$ around 0.2, stained with SYTO 9, washed three times, and spiked into 1 mL human whole blood. The final concentration of the bacteria ranged from $8 \times 10^3$ to $8 \times 10^6$ cfu/mL. The sample was centrifuged for 3 min at $200 \times g$ to remove the majority of the blood cells. The plasma (∼400 μL) was transferred to another tube and 1 mL Triton X-100 (1% in MH broth medium) was added to lyse the remaining blood cells and debris. The sample was incubated for 2 min at 37 °C and then centrifuged for 3 min at $1{,}000 \times g$. The supernatant was removed and 1.5 mL IGEPAL CA-630 (1% in MH broth medium) was added. The sample was incubated for 2 min at 37 °C and then centrifuged for 3 min at $1{,}000 \times g$. The supernatant was carefully removed and the 20-μL sample was loaded into the channel.

**ACKNOWLEDGMENTS.** This work is supported by the US Defense Threat Reduction Agency (DTRA) Grant (HDTRA114-AMD1) and the Penn State Research Fund. J.C.L. and K.E.M. were supported by NIH National Institute of Allergy and Infectious Diseases Grant (R01AI117032). However, any opinions, findings, conclusions, or other recommendations expressed herein are those of the authors and do not necessarily reflect the views of the US DTRA.

1. Zowawi HM, et al. (2015) The emerging threat of multidrug-resistant Gram-negative bacteria in urology. *Nat Rev Urol* 12:570–584.
2. Anonymous (2015) *Global Antimicrobial Resistance Surveillance System—Manual for Early Implementation* (WHO, Geneva, Switzerland).
3. Anonymous (2013) *Antibiotic Resistance Threats in the United States* (Centers for Disease Control and Prevention, Atlanta, GA).
4. Brook I, Wexler HM, Goldstein EJC (2013) Antianaerobic antimicrobials: Spectrum and susceptibility testing. *Clin Microbiol Rev* 26:526–546.
5. Pulido MR, García-Quintanilla M, Martín-Peña R, Cisneros JM, McConnell MJ (2013) Progress on the development of rapid methods for antimicrobial susceptibility testing. *J Antimicrob Chemother* 68:2710–2717.
6. Jorgensen JH, Ferraro MJ (2009) Antimicrobial susceptibility testing: A review of general principles and contemporary practices. *Clin Infect Dis* 49:1749–1755.
7. Davenport M, et al. (2017) New and developing diagnostic technologies for urinary tract infections. *Nat Rev Urol* 14:296–310.
8. Mach KE, Wong PK, Liao JC (2011) Biosensor diagnosis of urinary tract infections: A path to better treatment? *Trends Pharmacol Sci* 32:330–336.
9. Blair JMA, Webber MA, Baylay AJ, Ogbolu DO, Piddock LJV (2015) Molecular mechanisms of antibiotic resistance. *Nat Rev Microbiol* 13:42–51.
10. Li Y, Yang X, Zhao W (2017) Emerging microtechnologies and automated systems for rapid bacterial identification and antibiotic susceptibility testing. *SLAS Technol* 22:585–608.
11. Sin MLY, Mach KE, Wong PK, Liao JC (2014) Advances and challenges in biosensor-based diagnosis of infectious diseases. *Expert Rev Mol Diagn* 14:225–244.
12. Bauer KA, Perez KK, Forrest GN, Goff DA (2014) Review of rapid diagnostic tests used by antimicrobial stewardship programs. *Clin Infect Dis* 59(Suppl 3):S134–S145.
13. Czilwik G, et al. (2015) Rapid and fully automated bacterial pathogen detection on a centrifugal-microfluidic LabDisk using highly sensitive nested PCR with integrated sample preparation. *Lab Chip* 15:3749–3759.
14. Park KS, et al. (2016) Rapid identification of health care-associated infections with an integrated fluorescence anisotropy system. *Sci Adv* 2:e1600300.
15. Zhu Y, et al. (2016) Sensitive and fast identification of bacteria in blood samples by immunoaffinity mass spectrometry for quick BSI diagnosis. *Chem Sci (Camb)* 7:2987–2995.
16. Machen A, Drake T, Wang YF (2014) Same day identification and full panel antimicrobial susceptibility testing of bacteria from positive blood culture bottles made possible by a combined lysis-filtration method with MALDI-TOF VITEK mass spectrometry and the VITEK2 system. *PLoS One* 9:e87870.
17. Li H, Lu Y, Wong PK (2018) Diffusion-reaction kinetics of microfluidic amperometric biosensors. *Lab Chip* 18:3086–3089.
18. Chen CH, et al. (2010) Antimicrobial susceptibility testing using high surface-to-volume ratio microchannels. *Anal Chem* 82:1012–1019.
19. Cira NJ, Ho JY, Dueck ME, Weibel DB (2012) A self-loading microfluidic device for determining the minimum inhibitory concentration of antibiotics. *Lab Chip* 12:1052–1059.
20. Kim KP, et al. (2010) In situ monitoring of antibiotic susceptibility of bacterial biofilms in a microfluidic device. *Lab Chip* 10:3296–3299.
21. Jiang C-Y, et al. (2016) High-Throughput single-cell cultivation on microfluidic streak plates. *Appl Environ Microbiol* 82:2210–2218.
22. Kadlec MW, You D, Liao JC, Wong PK (2014) A cell phone-based microphotometric system for rapid antimicrobial susceptibility testing. *J Lab Autom* 19:258–266.
23. Avesar J, et al. (2017) Rapid phenotypic antimicrobial susceptibility testing using nanoliter arrays. *Proc Natl Acad Sci USA* 114:E5787–E5795.
24. Besant JD, Sargent EH, Kelley SO (2015) Rapid electrochemical phenotypic profiling of antibiotic-resistant bacteria. *Lab Chip* 15:2799–2807.
25. Zhu C, Yang Q, Liu L, Wang S (2011) Rapid, simple, and high-throughput antimicrobial susceptibility testing and antibiotics screening. *Angew Chem Int Ed Engl* 50:9607–9610.
26. Carey JR, et al. (2011) Rapid identification of bacteria with a disposable colorimetric sensing array. *J Am Chem Soc* 133:7571–7576.
27. Liu T, Lu Y, Gau V, Liao JC, Wong PK (2014) Rapid antimicrobial susceptibility testing with electrokinetics enhanced biosensors for diagnosis of acute bacterial infections. *Ann Biomed Eng* 42:2314–2321.

28. Mach KE, et al. (2011) A biosensor platform for rapid antimicrobial susceptibility testing directly from clinical samples. *J Urol* 185:148–153.
29. Schoepp NG, et al. (2017) Rapid pathogen-specific phenotypic antibiotic susceptibility testing using digital LAMP quantification in clinical samples. *Sci Transl Med* 9: eaal3693.
30. Dou M, Dominguez DC, Li X, Sanchez J, Scott G (2014) A versatile PDMS/paper hybrid microfluidic platform for sensitive infectious disease diagnosis. *Anal Chem* 86:7978–7986.
31. Syal K, et al. (2016) Antimicrobial susceptibility test with plasmonic imaging and tracking of single bacterial motions on nanometer scale. *ACS Nano* 10:845–852.
32. Longo G, et al. (2013) Rapid detection of bacterial resistance to antibiotics using AFM cantilevers as nanomechanical sensors. *Nat Nanotechnol* 8:522–526.
33. Tang Y, Zhen L, Liu J, Wu J (2013) Rapid antibiotic susceptibility testing in a microfluidic pH sensor. *Anal Chem* 85:2787–2794.
34. Kaushik AM, et al. (2017) Accelerating bacterial growth detection and antimicrobial susceptibility assessment in integrated picoliter droplet platform. *Biosens Bioelectron* 97:260–266.
35. Boedicker JQ, Li L, Kline TR, Ismagilov RF (2008) Detecting bacteria and determining their susceptibility to antibiotics by stochastic confinement in nanoliter droplets using plug-based microfluidics. *Lab Chip* 8:1265–1272.
36. Choi J, et al. (2013) Rapid antibiotic susceptibility testing by tracking single cell growth in a microfluidic agarose channel system. *Lab Chip* 13:280–287.
37. Choi J, et al. (2014) A rapid antimicrobial susceptibility test based on single-cell morphological analysis. *Sci Transl Med* 6:267ra174.
38. Peitz I, van Leeuwen R (2010) Single-cell bacteria growth monitoring by automated DEP-facilitated image analysis. *Lab Chip* 10:2944–2951.
39. Chung C-Y, Wang J-C, Chuang H-S (2016) Rapid bead-based antimicrobial susceptibility testing by optical diffusometry. *PLoS One* 11:e0148864.
40. Lu Y, et al. (2013) Single cell antimicrobial susceptibility testing by confined microchannels and electrokinetic loading. *Anal Chem* 85:3971–3976.
41. Baltekin Ö, Boucharin A, Tano E, Andersson DI, Elf J (2017) Antibiotic susceptibility testing in less than 30 min using direct single-cell imaging. *Proc Natl Acad Sci USA* 114: 9170–9175.
42. Dupnik K (2017) Queuing up for resistance testing. *Sci Transl Med* 9:eaao6118.
43. Anonymous (2012) *Methods for Dilution Antimicrobial Susceptibility Tests for Bacteria That Grow Aerobically; Approved Standard-Ninth Edition, CLSI M07-A9* (Clinical and Laboratory Standards Institute, Wayne, PA).
44. Golchin SA, Stratford J, Curry RJ, McFadden J (2012) A microfluidic system for long-term time-lapse microscopy studies of mycobacteria. *Tuberculosis (Edinb)* 92:489–496.
45. Anonymous (2015) *Performance Standards for Antimicrobial Susceptibility Testing; Twenty-Fifth Informational Supplement. CLSI M100-S25* (Clinical and Laboratory Standards Institute, Wayne, PA).
46. Patterson CA, Bishop MA, Pack JD, Cook AK, Lawhon SD (2016) Effects of processing delay, temperature, and transport tube type on results of quantitative bacterial culture of canine urine. *J Am Vet Med Assoc* 248:183–187.
47. Rowlands M, et al. (2011) The effect of boric acid on bacterial culture of canine and feline urine. *J Small Anim Pract* 52:510–514.